JOURNAL OF SPACECRAFT AND ROCKETS
Vol. 35, No. 2, March–April 1998

Autonomous Modal Identification of the Space Shuttle Tail Rudder

Richard S. Pappa*
NASA Langley Research Center, Hampton, Virginia 23681
and
George H. James III† and David C. Zimmerman‡
University of Houston, Houston, Texas 77204

Autonomous modal identification automates the calculation from experimental data of natural vibration frequencies, damping, and mode shapes of a structure. This technology complements damage detection techniques that use continuous or periodic monitoring of vibration characteristics. The approach incorporates the Eigensystem Realization Algorithm as a data analysis engine and an autonomous supervisor to condense multiple estimates of modal parameters using the consistent-mode indicator and correlation of mode shapes. The procedure was applied to free-decay responses of a Space Shuttle tail rudder and successfully identified the first seven vibration modes of the structure. The final modal parameters are a condensed set of results for 87 individual cases requiring approximately 5 min of computer time on a Unix workstation.

Introduction

MODAL identification is the process of calculating natural frequencies, damping, and mode shapes (modal parameters) from experimental data. In most cases the experimental data are free-decay vibration measurements, frequency response functions (FRFs), or impulse response functions (IRFs) obtained by inverse Fourier transformation of FRFs or by using the Observer–Kalman Filter Identification technique.[1] The Eigensystem Realization Algorithm (ERA) identifies structural modal parameters from IRFs or free-decay data. It is a multi-input/multi-output, time-domain technique that efficiently identifies many modes simultaneously, including closely spaced and weakly excited modes.[2]

ERA often generates good results using the default values of various algorithm parameters. However, depending on accuracy requirements, improvement of results may be necessary or desirable. One approach to improving modal identification results is to perform additional ERA analyses of the same data set(s) using other values of the algorithm parameters. For example, the data record length may be increased to improve the accuracy of linear, lightly damped, low-frequency modes (probably at the expense of other modes with higher nonlinearity, damping, or frequency). The extent to which modal identification results fluctuate with changes in algorithm parameters depends on the dynamic complexity of the structure, notably its modal density and degree of nonlinearity, and on the quality of the experimental measurements.

Autonomous modal identification of structures is a new technology in its early stages of development. In a previous study, autonomous modal identification was implemented using sliding-bandwidth filtering and both single-input and multi-input analyses.[3] In the present study, the size of the ERA Hankel data matrix and the assumed number of modes are varied. These are two additional, principal algorithm parameters. As more experience is gained with autonomous modal identification, a larger number of parameters will be included in the procedure. A full implementation eventually will incorporate all ERA algorithm parameters.

Received June 30, 1997; revision received Nov. 11, 1997; accepted for publication Nov. 15, 1997.

*Research Engineer, Structural Dynamics Branch, Structures Division.
†Visiting Research Engineer (from Sandia National Laboratories), Department of Mechanical Engineering. Member AIAA.
‡Associate Professor, Department of Mechanical Engineering.

In recent years, considerable attention has been given to the topic of damage detection in structures by use of vibration measurements.[4–7] This technology applies to a wide range of structures, including spacecraft, aircraft, buildings, bridges, offshore oil platforms, and wind turbines. Many of the methods under development detect damage by monitoring changes in modal parameters. Using modal parameters for this purpose is attractive for the following reasons: 1) Modal parameters change (to some degree) with any change in the mass, stiffness, or damping of the structure; 2) damage at inaccessible locations can be detected by changes in modal parameters measured at accessible locations; and 3) modal testing is a widely used, mature technology. The capability of generating structural modal parameters autonomously, i.e., without human involvement, for damage detection is the primary motivation for this work.

The next section describes the test article for this study and the manner in which it was tested in the laboratory. The following section summarizes the autonomous modal identification technique. The remainder of the paper shows principal identification results, including a summary of the final, condensed set of modal parameters.

Test Article and Test Description

Figure 1 shows the rudder/speed brakes (RSBs) of the Space Shuttle Orbiter. There are two pairs of RSBs, an upper pair and a lower pair. Each pair contains left and right surfaces that rotate in the same direction when used as a rudder and in opposite directions when used as a speed brake. The surfaces rotate up to ±27 deg as a rudder, individually up to 49 deg as a speed brake, or combined for joint rudder/speed-brake control. The vertical tail structure is covered with reusable thermal insulation and is designed to withstand a 163-dB acoustic environment with a maximum temperature of 350°F.

The structure is shown in Fig. 2. It is an upper-right RSB and was tested with free-free boundary conditions by suspending it from the actuator attach points using springs and cables. The test occurred at the NASA Johnson Space Center (JSC) in December 1996. This structure is one component of a circa-1980 Vertical Stabilizer Assembly (VSA) being used at JSC and the University of Houston for finite element model correlation and damage identification studies. The VSA originally served as an acoustic and static fatigue test article. The components of the VSA are being tested individually and assembled to develop techniques for correlating component and assembled models. The structure then will be damaged in various ways to test damage identification methods. The RSB is approximately $48 \times 7 \times 120$ in. and weighs 180 lb.

Figure 3 shows the excitation and response degrees of freedom used in the modal test. The structure was excited several times at each

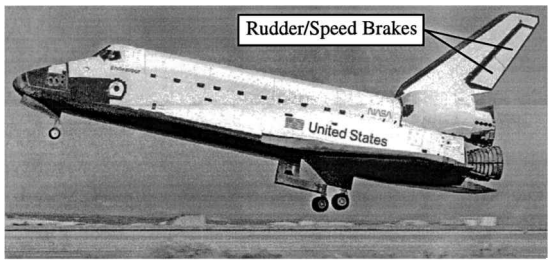

Fig. 1 Space Shuttle Orbiter.

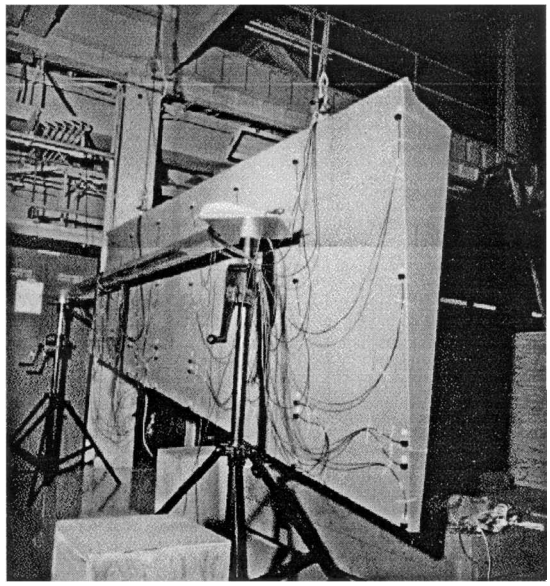

Fig. 2 Modal test configuration.

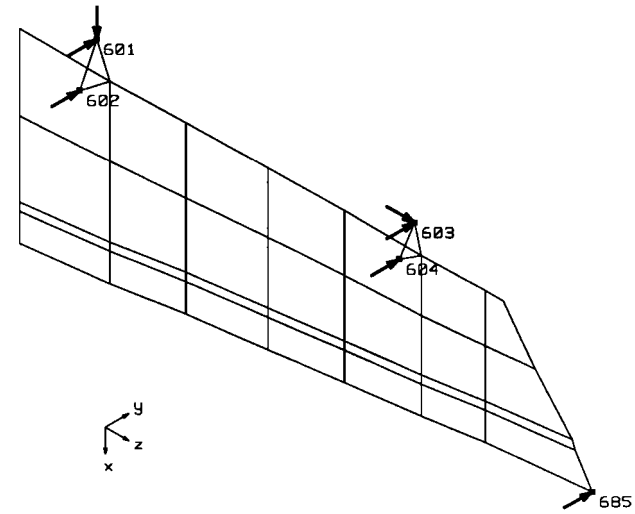

a) Seven impact locations

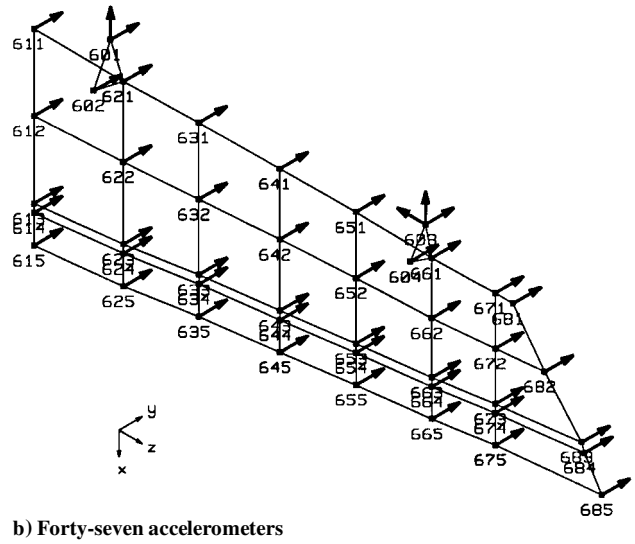

b) Forty-seven accelerometers

Fig. 3 Excitation and response locations.

of the seven locations shown in Fig. 3a with a force-instrumented hammer, and FRFs were calculated between the applied forces and each of the 47 accelerometers shown in Fig. 3b. Note that most of the impacts and response measurements are in the y direction (perpendicular to the surface of the structure), which emphasizes the primary, out-of-plane bending and torsional modes of the structure. In addition to calculating FRFs, the free-decay vibration responses for the final impact at each excitation location were recorded. The autonomous modal identification will analyze these free-decay responses.

Typical free-decay measurements and their corresponding fast Fourier transform (FFT) magnitude spectra appear in Fig. 4. Each time history contains 2033 data points at a sampling rate of 800 samples/s, and the data are alias-free out to a frequency of 312.5 Hz. The relatively noisy data in Fig. 4a are representative of most measurements obtained using y-direction excitation at actuator attach points 601–604. The cleaner data in Fig. 4b are representative of most measurements obtained using y-direction excitation at the apex of the structure (point 685). Although not shown, most measurements obtained using x- and z-direction excitation at points 601 and 603, respectively, are even noisier than those shown in Fig. 4a. The autonomous modal identification will analyze all 329 response measurements simultaneously to obtain global estimates of the modal parameters (329 responses = 47 accelerometers × 7 impact locations). By using all data simultaneously in the analysis, the cleaner measurements tend to dominate in the calculations over the noisier measurements because of their larger amplitudes.

Figure 5 shows the average power spectrum of all 329 free-decay responses. It provides a good overview of the natural frequencies of the structure and their relative strengths in the measurements. This function is the average squared magnitude of all FFT spectra such as shown on the right-hand sides of Figs. 4a and 4b. It indicates that there are seven predominant modes of the structure from 0 to 250 Hz (the frequency range of interest). There is also a small inflection in Fig. 5 at 72 Hz, indicating an additional mode in this frequency range, but it is too poorly excited and/or too poorly sensed to be accurately identified. The peak at 72 Hz is more apparent in other individual spectra not shown. This mode is probably a local mode of the cable suspension system.

Autonomous Modal Identification

Figure 6 is a flow diagram of the autonomous modal identification approach. There are four principal steps: 1) running the ERA[2,8]; 2) applying to the results thresholds that filter out unreasonable values; 3) condensing, i.e., reconciling, the most recent set of candidate modal parameters (the output of the thresholding step) with results obtained in previous passes around the feedback loop shown in Fig. 6; and 4) selecting appropriate algorithm parameters for the next ERA analysis.

Note that the mode condensation block is also known as the supervisor because it is responsible for determining how multiple ERA analyses are combined into a coherent, overall set of results. The final set of modal parameters is the last-computed output of the mode condensation process. The following paragraphs discuss each of the four steps in more detail.

ERA

ERA serves as a data analysis engine. It is a well-established, documented procedure for estimating structural modal parameters (natural frequencies, modal damping, and mode shapes) from free-decay vibration responses (or IRFs) based on a set of user-specified algorithm parameters.[8] Although default values and/or guidelines are available for each algorithm parameter, users have considerable

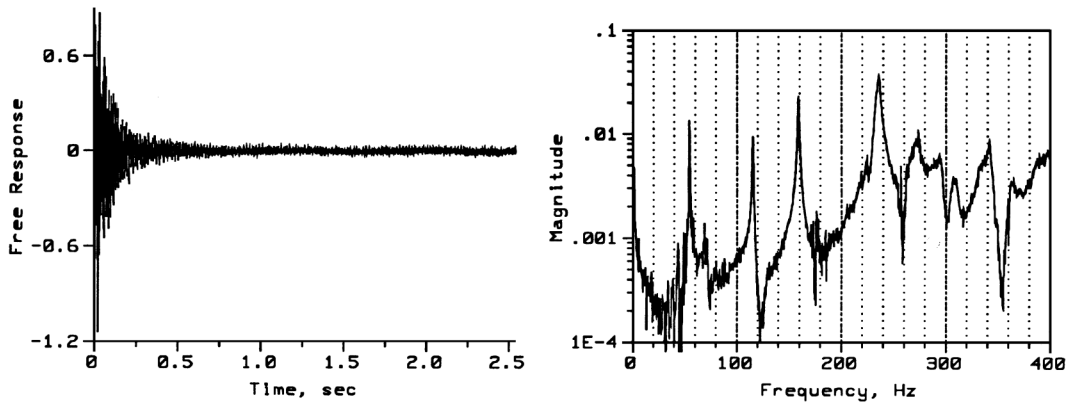

a) Excitation = 603*y*, response = 672*y*

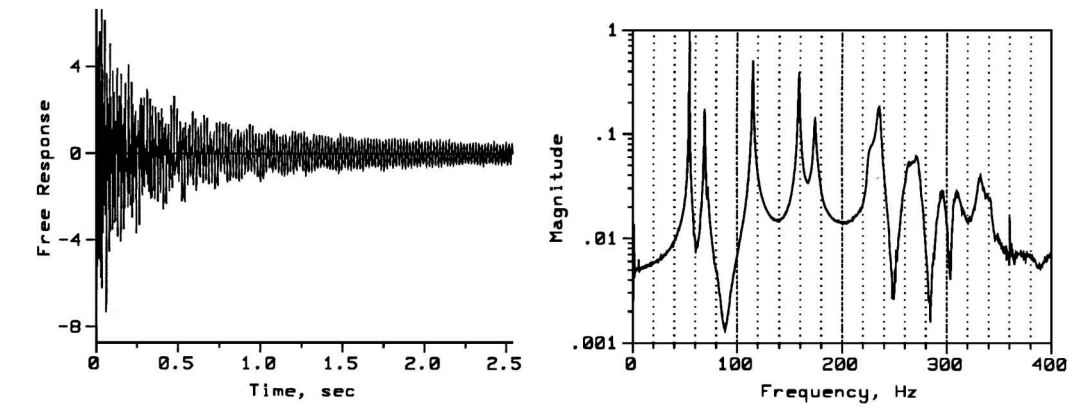

b) Excitation = 685*y*, response = 611*y*

Fig. 4 Typical free-decay responses and spectra.

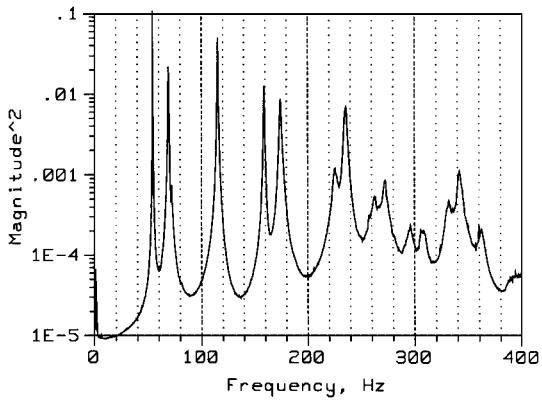

Fig. 5 Average power spectrum.

freedom in selecting their values. With experimental data, the ERA results will fluctuate to some degree with any change in the algorithm parameters. The magnitude of fluctuation varies from mode to mode, and it depends in a complex manner on the characteristics and quality of the data, including their modal density, degree of nonlinearity, noise level, modal response amplitude, damping level, spatial linear independence of closely spaced modes, sampling frequency, etc.

In addition to generating modal parameters, ERA calculates various accuracy indicators associated with each result. The principal accuracy indicator is the consistent-mode indicator (CMI), which provides a single, overall value for each mode, ranging from 0 to 100% (Ref. 9). Modes with CMI values greater than approximately 80% are identified with high confidence. Modes with values from 80 to 1% display moderate to large uncertainty. Extraneous "noise modes" have values of approximately zero. The CMI calculation uses both the temporal and the spatial consistency of the results, and it is a robust, proven indicator of modal identification accuracy.

Thresholding

The thresholding step in Fig. 6 eliminates unfeasible modal identification results generated by ERA. A normal characteristic of ERA is that it generates extra, nonphysical modes in addition to the true, structural modes. The noise modes mentioned in the preceding paragraph usually comprise a large fraction of these nonphysical modes. For good results with experimental data, at least half of the total number of identified modes normally will be nonphysical modes. Currently, nonphysical modes are eliminated from the results using the simple criteria shown in Fig. 7. Note that the CMI cutoff of 50% will allow some real, structural modes with poor accuracy to be deleted, but this is acceptable in most cases. (Ideally, that mode is identified better in another ERA analysis.) The damping and frequency cutoffs of 10 and 1%, respectively, are good selections for typical engineering structures having modal damping ratios on the order of 2% or less. These values would have to be increased for structures with higher levels of modal damping.

Mode Condensation (Supervisor)

Figure 8 shows the mode condensation logic, which is presently the principal autonomous aspect of the procedure. Mode condensation selects the best estimate of each structural mode from multiple estimates of the mode. In other words, given a set of best estimates of the modal parameters (a set that is available initially after the first pass through the loop of Fig. 6), mode condensation decides whether new estimates of the modal parameters (referred to as set 1 in Fig. 8) will be added to or will replace results already in the best set (referred to as set 2).

Mode condensation consists of the following steps.

1) For each mode in set 1 (mode n), compare its frequency with the frequencies of all modes in set 2. If there are no modes of set 2

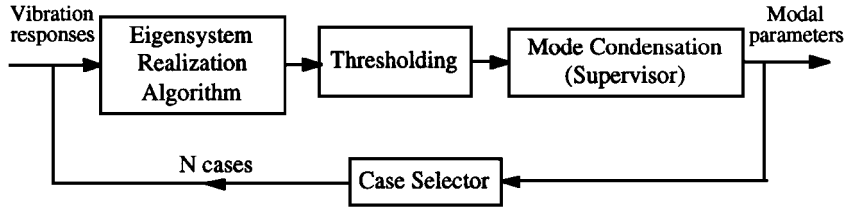

Fig. 6 Autonomous modal identification approach.

Delete modes with:

CMI < 50%, Damping < 0 or > 10%, or Frequency within 1% of edges of analysis bandwidth.

Fig. 7 Thresholding logic.

within 10% in frequency of mode n, add mode n to set 2. Recall that mode n has already passed through the thresholding step, and so it is probably a true, structural mode (albeit with some inaccuracy if its CMI value is not high).

2) For each mode of set 2 within 10% in frequency of mode n, calculate the modal assurance criterion (MAC).[10] MAC is the square of the correlation coefficient of the two modal vectors (mode shapes) and measures the similarity of mode shapes. If all MAC values are less than 70%, add mode n to set 2 because its mode shape is significantly different from all modes in set 2 with similar frequency.

3) If there are one or more MAC values of 70% or greater, select the mode in set 2 having the highest MAC (mode m), and compare its CMI value with the CMI of mode n. If the CMI of mode n (the new mode) is greater than that of mode m, replace mode m in set 2 with mode n.

Information generated during the mode condensation activity eventually will be used to recommend algorithm parameters for subsequent ERA analyses. A large amount of information concerning the characteristics of the data (such as the linear independence of closely spaced modes) is obtained during mode condensation, and this information could be used to select better algorithm parameters. This capability is under development and is not yet available.

Case Selector

The final block in Fig. 6 is the case selector. Because the RSB test article is a relatively simple structure, the case selection logic shown in Fig. 9 proved to be adequate for this application. Set A is a standard, default type of initial ERA analysis. Although it involves 35 cases, the total execution time is quite short (approximately 75 s) because the Hankel matrix and the number of measurements are fairly small. The final results of set A (discussed in the next section) contained two modes with CMI values less than 90% (out of a total of seven modes below 250 Hz). Accordingly, set B then was executed in an attempt to improve the accuracy of these modes. After both sets A and B were completed, set C combined the two groups of results into a final, overall set of results using the mode condensation logic of Fig. 8.

Sets A and B are multi-input/multi-output (MIMO) analyses using all 329 free-decay response measurements simultaneously. Both sets use a Hankel data matrix with 470 rows (10 shifts of the 47 outputs). However, the number of columns in the matrix increases from 70 in set A (10 shifts of the 7 inputs) up to 105 in set B (15 shifts of the 7 inputs). The maximum number of identified modes in any ERA analysis is always equal to one-half the minimum dimension of the Hankel matrix. For good results with experimental data, the maximum number of identified modes is typically in the range of approximately 2 to 10 times the number of structural modes in the data bandwidth (up to 400 Hz in this problem). The numbers of columns in sets A and B (70 and 105, respectively) were chosen on the basis of an estimated number of structural modes from 0 to 400 Hz of approximately 15 obtained by counting the peaks in the average power spectrum (Fig. 5).

Modal Identification Results

Natural Frequencies and CMI

Figures 10a and 10b show the ERA-identified natural frequencies between 0 and 250 Hz (the frequency range of interest) as a function of the assumed number of modes for sets A and B, respectively. There are seven predominant modes of the structure in this frequency range, as indicated. Each row of results in Fig. 10 corresponds to a separate ERA analysis with the specified number of assumed modes. Each identified mode is represented by a short vertical dash at the associated frequency. The height and width of each dash express the confidence of the result based on the CMI,[9] as described in the following paragraph. Note that these natural frequency results occur prior to the thresholding block of Fig. 6. For clarity, modes with CMI values less than 1% are not shown.

The height of each vertical dash in Fig. 10 is directly proportional to the CMI value such that a mode with a value of 100% has a vertical-dash height equal to the distance between y-axis tick marks. The width of each dash also increases with increasing CMI. This is done by using four linewidths ranging from narrowest to widest for the following ranges of CMI: 1) below 80%, 2) from 80 to 90%, 3) from 90 to 95%, and 4) above 95%. (On a computer terminal, the four linewidths correspond to four different colors, rather than linewidths, to differentiate results for closely spaced frequencies.)

The CMI accuracy indicator did an excellent job of distinguishing the true, structural modes from the nonphysical, computational modes generated by ERA. Figure 11 shows typical results from set A. These are the values for the top row of results in Fig. 10a. The seven structural modes have values that are consistently much higher than those of the nonphysical modes. In fact, nearly all nonphysical modes have CMI of less than 1% in this application. The unusually high value near 0 Hz is due to small dc offsets in the data. The other unusually high value at approximately 170 Hz is probably a local mode of the cable suspension system.

Although CMI clearly distinguishes the seven structural modes from the nonphysical modes, a close examination of Fig. 10 shows considerable variations of CMI for most of the structural modes as a function of the assumed number of modes (indicated by varying linewidths). Out of the 14 structural-mode results shown in Figs. 10a and 10b, only modes 2 and 3 in Fig. 10b have uniformly increasing CMI with increasing numbers of assumed modes. This desirable, convergent behavior occurs for well-excited, linear modes when the Hankel matrix size is large enough. On the other hand, all other results in Fig. 10 display fluctuating CMI values as the assumed number of modes increases. Unfortunately, such fluctuations are the rule rather than the exception with many experimental data sets because of unavoidable real-world effects, particularly nonlinearity and noise. The thresholding and mode condensation logic discussed earlier are designed to sift through the results of these 87 cases and extract the set of structural modal parameters having the highest confidence.

Mode Condensation Results

As indicated in Fig. 6, the final set of modal parameters from the autonomous modal identification approach is the output of the mode condensation process at the end of each case. If a sufficient collection of cases is run, the final, condensed set of modal parameters will be the best estimates of the true structural modes and nothing else.

This autonomous modal identification approach performed extremely well in this application. Figure 12 shows the number of identified modes, i.e., the number of modes in the final, condensed set, at the end of each case for set B. The results for set A are similar.

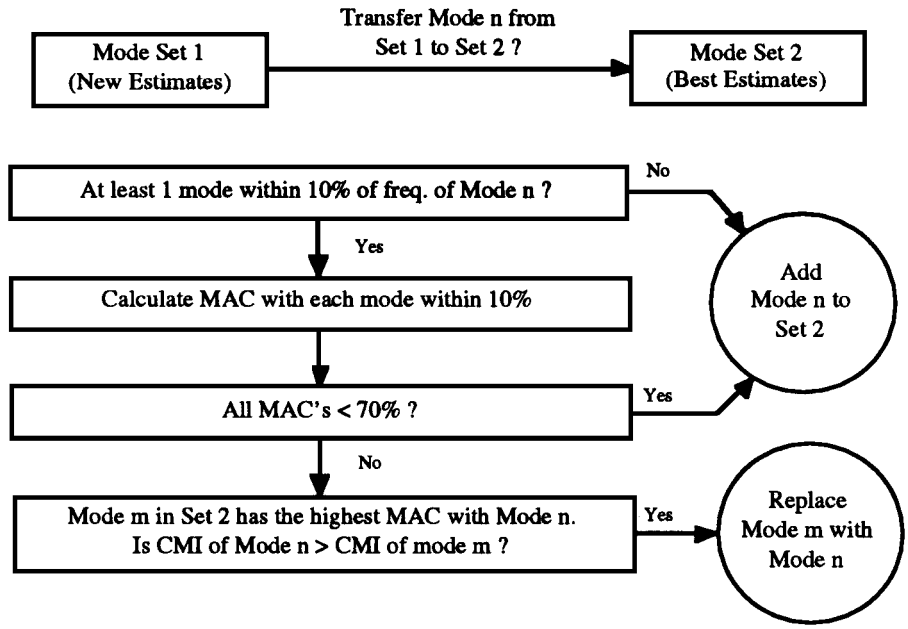

Fig. 8 Mode condensation logic.

Set A (35 cases): 47 x 7 MIMO analysis with Hankel matrix of 470 rows x 70 cols, Assumed No. of Modes - 1 through 35.

Stop here if all modes in the final results of Set A have CMI > = 90%. If not, proceed to Sets B and C.

Set B (52 cases): 47 x 7 MIMO analysis with Hankel matrix of 470 rows x 105 cols, Assumed No. of Modes - 1 through 52.

Set C: Overall Results - Combine results of Sets A and B by mode condensation.

Fig. 9 Case selector logic.

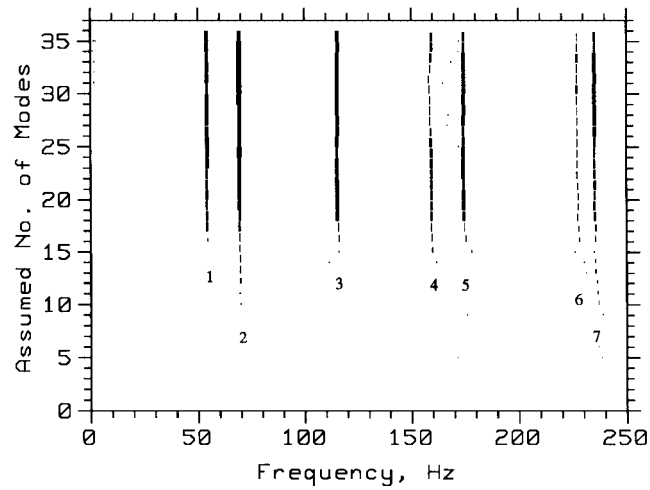

a) Set A (35 cases): Hankel matrix size = 470 rows × 70 columns

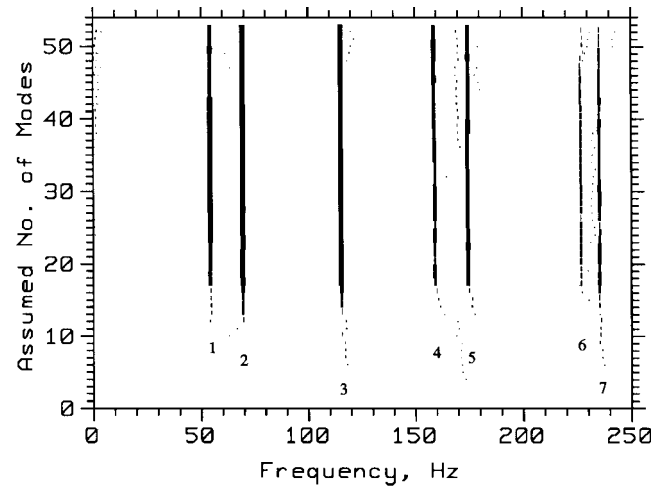

b) Set B (52 cases): Hankel matrix size = 470 rows × 105 columns

Fig. 10 Identified frequencies vs assumed number of modes.

Recall from Fig. 9 that individual results are obtained for sets A and B, which are then combined in set C using a final mode condensation. The dips in Fig. 12 show that modes are being replaced according to the logic of Fig. 8. At each abscissa value, the larger of the two numbers is the total number of modes in set 2 at the completion of the case. The smaller of the two numbers is the number of modes retained from the previous case. In other words, the difference between the two numbers is the number of modes replaced as a result of the ERA analysis for the particular case number. The total number of identified modes in both sets A and B steadily increased up to the true value of seven, with many fluctuations along the way indicating continuous improvement of results. This convergent behavior with continuous improvement of the results is how autonomous modal identification should operate.

Final Modal Identification Results

The final set of results for both sets A and B consisted of estimates of the seven true structural modes. Both sets converged to a stable number of modes, i.e., the replacement of modes slowed down and then ceased entirely as the case number approached 35 in set A and 52 in set B. Following completion of sets A and B, set C executed a final mode condensation on the two individual sets of results.

Table 1 shows the overall modal identification results obtained in set C. Column 2 gives the case number and set from which the result was obtained. Note that six of the seven modes came from

Table 1 Final modal parameters and accuracy indicators (set C)

Mode no.	Case no. (set)	Frequency, Hz	Damping factor, %	CMI, %	MPC-W,[a] %
1	31(B)	54.3	0.17	97.24	99.94
2	44(B)	69.3	0.59	98.52	99.99
3	26(B)	115.3	0.35	98.77	99.94
4	45(B)	158.8	0.28	96.13	99.92
5	48(B)	174.6	0.73	95.53	99.58
6	42(B)	226.6	1.12	87.61	98.68
7	28(A)	235.3	0.61	91.96	95.89

[a]Weighted modal-phase collinearity.

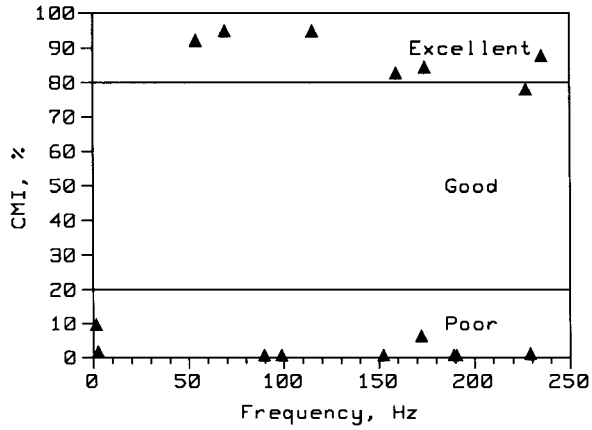

Fig. 11 Typical distribution of CMI values.

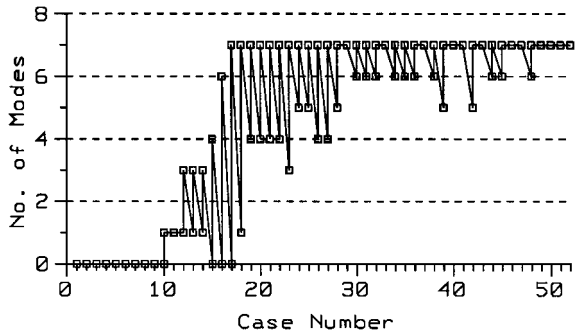

Fig. 12 Number of identified modes vs case number for set B.

set B, which used a larger Hankel data matrix than set A. In many cases, though not always, increasing the size of the ERA Hankel matrix will increase modal identification accuracy. However, there is a disproportionate increase in the computation time. For example, in this application, set A required 75 s of CPU time on an Alpha Unix workstation, whereas set B required 213 s of CPU time but achieved higher accuracy in many of the modes.

All of the CMI values in Table 1 are greater than 80%, indicating high confidence in the results. Furthermore, five of the CMI values are above 95%, indicating extremely high confidence in these modes. The right-hand column in Table 1 also gives the weighted modal-phase collinearity, which is a parameter used in the CMI calculation.[9] MPC-W measures the nearness of the mode shape to a monophase vector, i.e., to a classical, normal mode. Values greater than 99% are extremely high.

Figures 13a–13g show the corresponding mode shapes. All seven of the modes are global, out-of-plane bending and torsional modes, as expected. Each mode has a well-defined, predictable shape, substantiating the accuracy of the results. Furthermore, all seven frequencies and mode shapes agree closely with another, independent set of results obtained by analyzing FRFs with the polyreference technique. Good correlation of the two independent sets of results provides additional confidence in the accuracy of the autonomous modal identification approach.

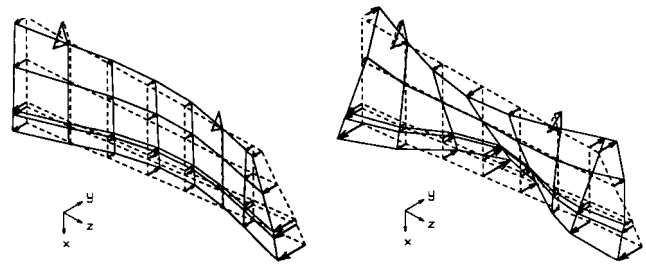

a) First bending at 54.3 Hz **d) Second torsion at 158.8 Hz**

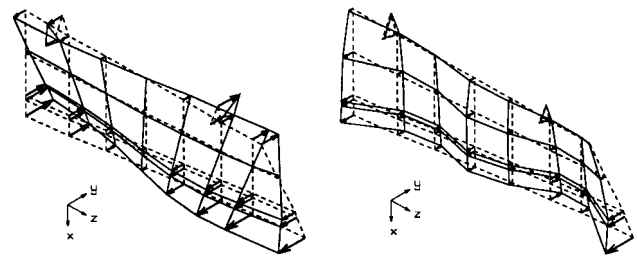

b) First torsion at 69.3 Hz **e) Third bending at 174.6 Hz**

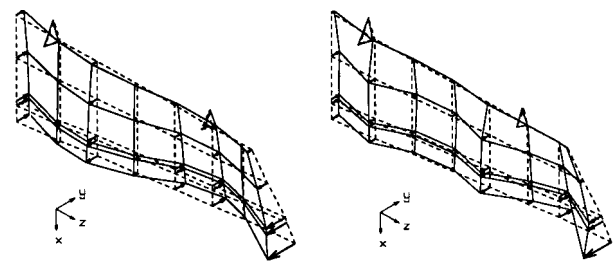

c) Second bending at 115.3 Hz **f) Fourth bending at 226.6 Hz**

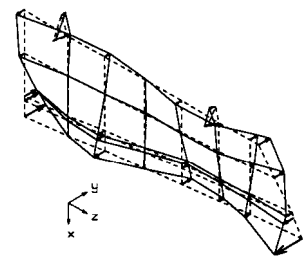

g) Third torsion at 235.3 Hz

Fig. 13 Mode shapes (set C: final results).

Conclusions

Considerable research is currently under way on several fronts in the area of damage detection in structures by use of changes in vibration characteristics. Many of the techniques under development require periodic calculation of structural modal parameters from experimental data. An attractive approach to this problem is autonomous modal identification. This new technology also promises improved speed and accuracy for more-traditional laboratory applications of modal identification techniques.

The autonomous modal identification approach described in this paper is a fairly straightforward extension of ERA. It successfully identified the seven vibration modes of the Shuttle Orbiter tail rudder from 0 to 250 Hz in approximately 5 min of computer time. As more experience is gained using this technology on a variety of other structures, additional logic and features will be added to the software to improve its performance and reliability in generating optimum modal parameters without human involvement.

Acknowledgment

The authors acknowledge the advice and assistance of Mike Grygier of the NASA Johnson Space Center, who serves as NASA Technical Monitor for the Vertical Stabilizer Assembly test program.

References

[1]Juang, J.-N., *Applied System Identification*, 1st ed., PTR Prentice–Hall, Englewood Cliffs, NJ, 1994, pp. 175–228.

[2]Juang, J.-N., and Pappa, R. S., "An Eigensystem Realization Algorithm for Modal Parameter Identification and Model Reduction," *Journal of Guidance, Control, and Dynamics*, Vol. 8, No. 5, 1985, pp. 620–627.

[3]Pappa, R. S., Woodard, S. E., and Juang, J.-N., "The Development of Autonomous Structural Modal Identification," *Sound and Vibration*, Vol. 31, No. 8, 1997, pp. 18–23.

[4]Grygier, M. S., "Modal Test Technology as Non-Destructive Evaluation of Space Shuttle Structures," *Dual-Use Space Technology Transfer Conference and Exhibition*, edited by K. Krishen, NASA CP-3263, 1994, pp. 329–334.

[5]James, G. H., III, "Development of Structural Health Monitoring Techniques Using Dynamics Testing," Sandia National Labs., Rept. SAND-96-0810, Albuquerque, NM, March 1996.

[6]Doebling, S. W., Farrar, C. R., Prime, M. B., and Shevitz, D. W., "Damage Identification and Health Monitoring of Structural and Mechanical Systems from Changes in Their Vibration Characteristics: A Literature Review," Los Alamos National Lab., Rept. LA-13070-MS, Los Alamos, NM, May 1996.

[7]Zimmerman, D. C., Smith, S. W., Kim, H.-M., and Bartkowicz, T. J., "An Experimental Study of Structural Damage Detection Using Incomplete Measurements," *Journal of Vibration and Acoustics*, Vol. 118, No. 4, 1996, pp. 543–550.

[8]Pappa, R. S., "Eigensystem Realization Algorithm User's Guide for VAX/VMS Computers," NASA TM-109066, 1994.

[9]Pappa, R. S., Elliott, K. B., and Schenk, A., "Consistent-Mode Indicator for the Eigensystem Realization Algorithm," *Journal of Guidance, Control, and Dynamics*, Vol. 16, No. 5, 1993, pp. 852–858.

[10]Allemang, R. J., and Brown, D. L., "A Correlation Coefficient for Modal Vector Analysis," *Proceedings of the 1st International Modal Analysis Conference* (Orlando, FL), Union College, Schenectady, NY, 1982, pp. 110–116.

R. B. Malla
Associate Editor